Performance Bounds for Tracking Multiple Objects using a Single UAV

Anders Albert
Department of Engineering Cybernetics
Norwegian University of Science and Technology
Trondheim, Norway
Email: anders.albert@ntnu.no

Lars Imsland
Department of Engineering Cybernetics
Norwegian University of Science and Technology
Trondheim, Norway
Email: lars.imsland@ntnu.no

Abstract—In this paper we calculate probabilistic estimates for the size of an area a single unmanned aerial vehicle (UAV) can expect to monitor when tracking multiple objects. The objects are assumed to move according to a linear velocity model with Gaussian process noise. We use a Kalman filter to estimate the position of the objects. By using the covariance matrix of the Kalman filter, we can derive the necessary visitation period for a UAV to have a probability within a given confidence interval of redetecting the object at the estimated position. Then, we use this visitation period to calculate the probabilistic estimate for the area a single UAV can monitor. We demonstrate the results in Monte Carlo simulations.

I. Introduction

Unmanned aerial vehicles (UAVs) have many applications both within military and civilian areas, and the number of applications are expected to increase in the years to come [1]. A classical research question relevant for many UAV applications, is searching and tracking objects (or sometimes called targets) using a single or multiple UAVs.

Examples of applications for searching and tracking of objects are: iceberg monitoring, fire detection and monitoring, border patrol, surveillance and reconnaissance, [2, 3, 4, 5].

The searching and tracking of objects (STO) can be viewed as a filtering problem. While most research within STO is concerned with path planning, the problem of finding performance bounds for filters have been less studied.

There are multiple alternatives for performance bounds on filters [6], but the most popular is the Posterior Cramér-Rao Lower Bond (PCRLB) first derived by Tichavsky et al. [7]. This is a mean-square error bound on state estimation error of general discrete-time systems, and the reason for its popularity is probably the low computational complexity of the bound [6]. PCRLB has been applied to multiple areas of research. For example path planning [8, 9, 10], and time horizon estimation [11].

Another approach that can be used to derive bounds on the performance of a STO problem is to combine the objectives of searching and object tracking into a single objective function [12, 13, 14] or divide them into multiple layer objective function like Tian et al. [15].

To our knowledge there have been no attempts to estimate the size of the area a UAV can expect to monitor based on the number and uncertainty of the objects in that area.

This estimate will be useful for allocating resources to STO problems. It will also provide a performance metric of how well any algorithm can expect to perform and can be used as a basis for designing new path planning algorithms.

We assume that a UAV is equipped with a sensor that has a given measurement frequency and accuracy.

A. Contribution

First, we give some simple results on the necessary visitation frequency for a single object to keep the error in position estimate within a given confidence interval. Second, we use a Monte Carlo approach to approximate probability distribution of traveling salesperson-(TSP) solutions given the number of objects to track. We then use the results for indicating how many objects/how large area can be monitored by a single UAV.

B. Organization

This paper is organized as follows. In Section II we introduce the model we use for the objects, the UAV and it's sensor. In addition, we also present the Kalman filter we use estimating the state of the objects and use as a basis for the derivations in Section III. The main result of this section is the necessary visitation frequency for a single object to keep the error in position estimate within a given confidence interval. In Section IV we approximate the probability distribution for the solution of TSPs given the number of objects. We use this to indicate how large area/how many object a single UAV can monitor. To demonstrate the result we run 100 simulations for a single UAV monitoring an area with the estimated size and count the number of times the objects are redetected and compare it to the number of times the error in position estimate gets outside the field of view (FOV) of the UAV in Section V. Finally, we give a conclusion and further work in Section VII.

C. Notation

Throughout this paper separate between scalars, vectors and matrices as follows. Scalar variables are written with lowercase letters. All vectors and matrices are denoted with bold lowercase and uppercase letters. In addition, the notation I and 0 will mean the 2×2 identity and zero matrices.

II. System Model and Kalman filter

We model the objects as particles moving with variable velocity described as a Gaussian random walk:

$$\dot{\boldsymbol{\xi}}_i = \begin{bmatrix} \dot{\boldsymbol{s}_i} \\ \dot{\boldsymbol{v}_i} \end{bmatrix} = \begin{bmatrix} \boldsymbol{0} & \boldsymbol{I} \\ \boldsymbol{0} & \boldsymbol{0} \end{bmatrix} \boldsymbol{\xi}_i + \begin{bmatrix} \boldsymbol{0} \\ \boldsymbol{I} \end{bmatrix} \boldsymbol{w}_i(t) \quad \forall i \in [1, \ldots, n_{\text{object}}]$$

(1)

where $\boldsymbol{\xi}_i = [\boldsymbol{s}_i, \boldsymbol{v}_i]^T$ is the state of each object consisting of Cartesian 2D coordinates, $\boldsymbol{s}_i \in \mathbb{R}^{1 \times 2}$, and velocity, $\boldsymbol{v}_i \in \mathbb{R}^{1 \times 2}$. The process noise, $\boldsymbol{w}_i(t)$, is assumed to be a Gaussian distribution with zero mean and variance $q_i \boldsymbol{I}$, $\boldsymbol{w}_i(t) \sim \mathcal{N}([\begin{matrix} 0 & 0 \end{matrix}]^T, q_i \boldsymbol{I})$.

The UAV is modeled as Dubins vehicle:

$$\dot{\boldsymbol{z}} = \begin{bmatrix} \dot{x} \\ \dot{y} \\ \dot{\psi} \end{bmatrix} = \begin{bmatrix} U \cos(\psi) \\ U \sin(\psi) \\ u \end{bmatrix}$$

(2)

$$-u_{\text{lim}} \le u \le u_{\text{lim}}$$

where $\boldsymbol{z}$ is the state of the UAV consisting of Cartesian coordinates, $(x, y)^T$, in addition to heading, ψ. The velocity, U, is assumed to be constant, and the turn rate, u, is bounded.

The UAV has a sensor to measure position of objects. The sensor can for example be a camera that takes a picture with a given frequency [16]. We assume the sensor obtains position measurements with a frequency $\frac{1}{\Delta T}[\frac{1}{s}]$,

$$\boldsymbol{y}_k = \{\boldsymbol{y} \quad |\boldsymbol{y} = [\begin{matrix} \boldsymbol{I} & \boldsymbol{0} \end{matrix}] \boldsymbol{\xi}_{i,k} + \boldsymbol{v}_k, \quad \forall \boldsymbol{\xi}_{i,k} \in \text{FOV}\}$$

(3)

where $\boldsymbol{y}_k$ is the set of position measurements obtained at timestep k, which can be empty or contain one or more measurements, corresponding to the number of objects within FOV. The state of object i at timestep k, $\boldsymbol{\xi}_{i,k}$, is the time discretized state from equation (1). Finally, the measurement has a Gaussian distributed noise $\boldsymbol{v}_k \sim \mathcal{N}([\begin{matrix} 0 & 0 \end{matrix}]^T, r\boldsymbol{I})$, where r is the variance. The notation $\boldsymbol{\xi}_{i,k} \in \text{FOV}$ means that object i is within field of view (FOV) the UAV at timestep k. We assume a circular FOV throughout this paper.

The Kalman filter is the optimal estimator for linear systems with Gaussian noise, (1) [17]. The procedure of a Kalman filter consists of two parts. First, it propagates the estimated state and associated covariance matrix. Second, it use the newest measurement and update the state estimate based on the certainty of the measurement, given by the variance, r. For our case, the second step is only performed when the UAV is observing the current object.

The a priori step of the discrete Kalman filter for each object (here the subscript i is dropped for clarity):

$$\hat{\boldsymbol{\xi}}_{k+1}^{\text{priori}} = \boldsymbol{A}\hat{\boldsymbol{\xi}}_k, \qquad \hat{\boldsymbol{\xi}}_0 = [\begin{matrix} \boldsymbol{y}_0 & 0 & 0 \end{matrix}]^T,$$

(4a)

$$\boldsymbol{P}_{k+1}^{\text{priori}} = \boldsymbol{A}\boldsymbol{P}_k\boldsymbol{A}^T + \boldsymbol{Q}, \quad \boldsymbol{P}_0 = \begin{bmatrix} r\boldsymbol{I} & \frac{r\sigma_{v,0}^2}{\Delta T}\boldsymbol{I} \\ \frac{r\sigma_{v,0}^2}{\Delta T}\boldsymbol{I} & \sigma_{v,0}^2\boldsymbol{I} \end{bmatrix},$$

(4b)

where

$$\boldsymbol{A} = \begin{bmatrix} \boldsymbol{I} & \Delta T\boldsymbol{I} \\ \boldsymbol{0} & \boldsymbol{I} \end{bmatrix}, \boldsymbol{Q} = \begin{bmatrix} \boldsymbol{0} & \boldsymbol{0} \\ \boldsymbol{0} & q\boldsymbol{I} \end{bmatrix}, \boldsymbol{R} = r\boldsymbol{I},$$

$$\sigma_{v,0}^2 = \frac{1}{12}(v_{\text{max}} - v_{\text{min}})^2$$

where $\hat{\boldsymbol{\xi}}$ is the estimated state of the object. The subscript $k+1$ and k denotes the next state and the current state. The superscript $priori$ indicates that this is the prediction step. The initial state estimates, $\hat{\boldsymbol{\xi}}_0$, is given by the first measurement, $\boldsymbol{y}_0$. The covariance matrix at timestep k is $\boldsymbol{P}_k$. The covariance of the process and measurement noise is $\boldsymbol{Q}$ and $\boldsymbol{R}$. The constants, q and r, are the same as in equation (1) and (3). The initial velocity variance is $\sigma_{v,0}^2$, where we have assumed a uniform distributed velocity of the objects with limits $[v_{\text{min}}, v_{\text{max}}]$. Finally, we use the sensor measurement frequency to set the step length, ΔT.

When a measurement is available, the posteriori step is performed (also here is the subscript i for each object dropped for clarity):

$$\boldsymbol{K} = \boldsymbol{P}_{k+1}^{\text{priori}}\boldsymbol{C}^T[(\boldsymbol{C}\boldsymbol{P}_{k+1}^{\text{priori}}\boldsymbol{C}^T + \boldsymbol{R})]^{-1}$$

(5a)

$$\hat{\boldsymbol{\xi}}_{k+1}^{\text{post}} = \hat{\boldsymbol{\xi}}_{k+1}^{\text{priori}} + \boldsymbol{K}(\boldsymbol{y}_k - \boldsymbol{C}\hat{\boldsymbol{\xi}}_{k+1}^{\text{priori}})$$

(5b)

$$\boldsymbol{P}_{k+1}^{\text{post}} = (\boldsymbol{I} - \boldsymbol{K}\boldsymbol{C})\boldsymbol{P}_{k+1}^{\text{priori}}$$

(5c)

where

$$\boldsymbol{C} = [\begin{matrix} \boldsymbol{I} & \boldsymbol{0} \end{matrix}]$$

here $\boldsymbol{K}$ is the Kalman gain, which calculates the weight to for the new measurement. The superscript $post$ is to indicate the update step. The remaining constants are the same as in equation (4).

III. Single Object Visitation Frequency

In this section we use the covariance matrix from the Kalman filter for a single object to calculate the necessary visitation frequency to keep the error in position estimate within a given confidence interval.

The Kalman filter gives an estimate for the position of each objects, but it also gives us a measure of the uncertainty in the estimate, the covariance matrix. When we study the equations for the objects (1), and the Kalman equation, (4)-(5), we notice that the covariance matrix will have the form:

$$\boldsymbol{P}_k = \begin{bmatrix} \sigma_{x,k}^2 & 0 & \sigma_{xv_x,k} & 0 \\ 0 & \sigma_{y,k}^2 & 0 & \sigma_{yv_y,k} \\ \sigma_{xv_x,k} & 0 & \sigma_{v_x,k}^2 & 0 \\ 0 & \sigma_{yv_y,k} & 0 & \sigma_{v_y,k}^2 \end{bmatrix}$$

(6)

where $\sigma_{x,k}^2$ and $\sigma_{y,k}^2$ are the variances in x- and y-direction at timestep k. The corresponding velocity variances are $\sigma_{v_x,k}^2$ and $\sigma_{v_y,k}^2$. In addition the covariance between the position and velocity in x- and y-direction are $\sigma_{xv_x,k}$ and $\sigma_{yv_y,k}$.

It is often reasonable to assume that $\sigma_y^2 = \sigma_x^2$, $\sigma_{yv_y} = \sigma_{xv_x}$, and $\sigma_{v_y}^2 = \sigma_{v_x}^2$. By implementing this in (6), the covariance matrix is defined by only three parameters.

The simple form for the covariance matrix in equation (6) is caused by the assumption what there is no coupling between the north/east position and velocity for the process and measurement noise defined by the covariance matrices Q and R.

This observation enable us to derive the following result.

Theorem 1 (Maximum position uncertainty). *Let ΔT be the period for sensor measurement frequency and FOV_{radius} be the radius (in meter) for the field of view of a UAV. Also assume that an object is characterized by the system modeled by equation (1), with process noise variance, q. If χ_2^2 is the p-value for a chi-squared distribution of two degrees of freedom, then the equation:*

$$\frac{1}{3}q\Delta T^3 n^3 + (\Delta T^2 \sigma_{v_x,k}^2 - \frac{1}{2}q\Delta T^3)n^2$$
$$+ (2\Delta T\sigma_{xv_x,k} + \frac{1}{6}q\Delta T^3)n + (\sigma_{x,k}^2 - \frac{FOV_{radius}^2}{\chi_2^2}) = 0 \tag{7}$$

will have exactly one real solution, denoted n_{real}. Here $\sigma_{x,k}$, $\sigma_{v_x,k}$, and $\sigma_{xv_x,k}$ are the elements the of covariance matrix P_k at time k, (6), for the position estimate of the object with initial condition given by equation (4b).

Then, if the UAV takes a measurement at the estimated position of the object given by equation (4a) at the time

$$T_{crit} = n_{real}\Delta T \tag{8}$$

it will have a probability of measuring the real position of the object within the confidence interval given by the p-value of the χ_2^2 distribution.

For example, if $\chi_2^2 = 5.99$ the UAV will have a 95% chance of finding the object within its field of view when taking a measurement at the estimated object position if it returns to the object after T_{crit} seconds.

Proof. Let P_k be the covariance matrix of the object at timestep k. Then, by applying equation (4b) multiple times we get the following (here we drop the superscript *priori* since we assume that the object is never observed):

$$P_{k+n} = A^n P_k (A^n)^T + \sum_{i=0}^{n-1} A^i Q (A^i)^T \tag{9}$$

here n is the number of steps into the future from time k. Since

$$A^n = \begin{bmatrix} I & n\Delta T I \\ 0 & I \end{bmatrix}. \tag{10}$$

we get

$$P_{k+n} = \begin{bmatrix} a_n I & b_n I \\ b_n I & c_n I \end{bmatrix} + q\Delta T \sum_{i=0}^{n-1} \begin{bmatrix} i^2(\Delta T)^2 I & i\Delta T I \\ i\Delta T I & I \end{bmatrix} \tag{11}$$

where

$$a_n = \sigma_{x,k}^2 + 2n\Delta T\sigma_{xv_x,k} + (n\Delta T)^2\sigma_{v_x,k}^2$$
$$b_n = \sigma_{xv_x,k} + n\Delta T\sigma_{v_x,k}^2$$
$$c_n = \sigma_{v_x,k}^2$$

By using formulas for the sums in the second part of (11), we get

$$P_{k+n} = \begin{bmatrix} a_n I & b_n I \\ b_n I & c_n I \end{bmatrix}$$
$$+ q\Delta T \begin{bmatrix} (\Delta T)^2(\frac{1}{3}n^3 - \frac{1}{2}n^2 + \frac{1}{6}n)I & \frac{1}{2}\Delta T(n^2 - n)I \\ \frac{1}{2}\Delta T(n^2 - n)I & nI \end{bmatrix} \tag{12}$$

The upper left corner is the position variance at timestep $k+n$

$$\sigma_{x,k+n}^2 = \frac{1}{3}q\Delta T^3 n^3 + (\Delta T^2\sigma_{v_x,k}^2 - \frac{1}{2}q\Delta T^3)n^2$$
$$+ (2\Delta T\sigma_{xv_x,k} + \frac{1}{6}q\Delta T^3)n + \sigma_{x,k}^2 \tag{13}$$

Let $\tilde{\xi}_{k+n} = \begin{bmatrix} \tilde{s}_{k+n} & \tilde{v}_{k+n} \end{bmatrix}$ be the error in state estimate for the object at $t_k + n\Delta T$ and $\tilde{s}_{k+n} = \begin{bmatrix} \tilde{x}_{k+n} & \tilde{y}_{k+n} \end{bmatrix}^T$ the error in position estimate. In addition, given a circular FOV of the UAV with a radius = FOV_{radius}. We need

$$|FOV_{radius}| \geq |\tilde{s}_{k+n}| \tag{14}$$
$$FOV_{radius}^2 \geq \tilde{x}_{k+n}^2 + \tilde{y}_{k+n}^2. \tag{15}$$

We know that both $\tilde{x}$ and $\tilde{y}$ are Gaussian distributed with zero mean and an increasing variance of $\sigma_{x,k+n}^2$. If we divide the expression by the variance we get the following:

$$(\frac{1}{\sigma_{x,k+n}^2})FOV_{radius}^2 \geq \frac{1}{\sigma_{x,k+n}^2}(\tilde{x}_{k+n}^2 + \tilde{y}_{k+n}^2) \tag{16}$$

If we look at the right side of equation (16) we have the sum of two normally distributed random variables squared. This is a chi-squared distribution of second order. We can calculate a confidence interval by using this distribution. Let χ_2^2 be the p-value of a given confidence interval. Then, the maximum value the variance can have without getting outside this confidence interval is

$$(\frac{1}{\sigma_{x,k+n}^2})FOV_{radius}^2 = \chi_2^2 \tag{17a}$$

$$\sigma_{x,k+n}^2 = \frac{FOV_{radius}^2}{\chi_2^2} \tag{17b}$$

We can now combine equation (13) and (17b) to get equation (7).

Furthermore, the equation (7) is a cubic function in n. If we let α, β, γ and δ be the constants defining this function, $\alpha n^3 + \beta n^2 + \gamma n + \delta = 0$. Then, the discriminant is given by

$$\Delta = 18\alpha\beta\gamma\delta - 4\beta^3\delta + \beta^2\gamma^2 - 4\alpha\gamma^3 - 27\alpha^2\delta^2 \tag{18}$$

When the discriminant is negative, the cubic function will have only one real and two complex conjugated solutions [18]. Since we must choose q, r, $\Delta T > 0$ and we use initial conditions given by equation (4b) the discriminant is always negative, and thus the cubic function in equation (7) will have only one real solution, n_{real}. $\square$

We now have the maximal value the position variance can reach. To get the necessary visitation frequency of an object, we need to know the minimum possible position variance. This limit depends on the measurement frequency and accuracy of the sensor, in addition to the process noise of the object.

We can calculate this limit by noticing that the covariance matrix will eventually reach a steady-state. If we combine the priori, (4), and the posteriori, (5), step into a single step with the object model, (1), and measurement model, (3), we get the following equation for the covariance matrix:

$$\boldsymbol{P}_{k+1}^{\text{post}} = \frac{1}{a_1 + r} \begin{bmatrix} ra_1\boldsymbol{I} & rb_1\boldsymbol{I} \\ rb_1\boldsymbol{I} & (-b_1^2 + (c_1 + \Delta Tq)(a_1 + r))\boldsymbol{I} \end{bmatrix} \tag{19}$$

where the constants a_1, b_1, and c_1 are given by (11).

The steady-state is reached when $\boldsymbol{P}_{k+1}^{\text{post}} = \boldsymbol{P}_k$. This corresponds to setting equation (19) equal to (6) with $[\sigma_{x,k}, \sigma_{xv_x,k}, \sigma_{v_x,k}] = [\sigma_{x,c}, \sigma_{xv_x,c}, \sigma_{v_x,c}]$, which gives the following set of equations:

$$\sigma_{x,c}^2 = \frac{ra_1}{a_1 + r} \tag{20a}$$

$$\sigma_{xv_x,c} = \frac{rb_1}{a_1 + r} \tag{20b}$$

$$\sigma_{v_x,c}^2 = \frac{-b_1^2}{a_1 + r} + c_1 + \Delta Tq \tag{20c}$$

This set of equations is easily solved, for instance with a Newton-method.

We can now derive the following result.

Theorem 2 (Object necessary visitation period). *Assume that each time a UAV visits an object it obtains a sufficient number of measurements for the covariance to reach the steady state defined by* (20). *Then, the necessary visitation period (NVP) for the object to guarantee detection for each visit within the confidence interval given by* χ_2^2 *is:*

$$T_{NVP} = n_{real}\Delta T \tag{21}$$

where n_{real} is the solution to equation (7) *in Theorem 1 with $\sigma_{x,k} = \sigma_{x,c}$, $\sigma_{xv_x,k} = \sigma_{xv_x,c}$, and $\sigma_{v_x,k} = \sigma_{v_x,c}$.*

Proof. We have assumed that each time the UAV visits an object the steady-state of the covariance is reached. Then, by theorem 1, the maximum position variance, $\sigma_{x,k}$, will never exceed the limit, $\frac{\text{FOV}_{radius}^2}{\chi_2^2}$. Since the error in position estimate is a chi-squared distribution, the probability of redetection will thus be given by the p-value, χ_2^2. $\square$

Theorem 2 gives us the necessary visitation period of an object. However, we assumed that the steady-state of the covariance will be reached each time an object is measured.

When the sensor of a UAV measures an object, the covariance matrix will converges exponentially fast towards the steady-state, but never reach it. This might seem like a problem. However, we can get arbitrary close to the steady-state by using a iterative method. The procedure is as follows.

First, use Theorem 2 to find $[\sigma_{x,c}, \sigma_{xv_x,c}, \sigma_{v_x,c}]$. Then, use Theorem 1 to calculate n_{real} and use it to find $[\sigma_{x,k+n}, \sigma_{xv_x,k+n}, \sigma_{v_x,k+n}]$ given by equation (13) and

$$\sigma_{xv_x,k+n} = \sigma_{xv_x,k} + n\Delta T\sigma_{v_x,k}^2 + \frac{1}{2}q(\Delta T)^2(n^2 - n) \tag{22a}$$

$$\sigma_{v_x,k+n}^2 = \sigma_{v_x,k}^2 + q\Delta Tn \tag{22b}$$

which can be found from reading the element (1,2) and (2,2) of the matrices in equation (12).

Finally, use an iterative method with equation (19) to find the number of iterations necessary to get within, the distance ϵ (measured in Euclidian distance), of the covariance matrix characterized by $[\sigma_{x,k+n}, \sigma_{xv_x,k+n}, \sigma_{v_x,k+n}]$ to $[\sigma_{x,c}, \sigma_{xv_x,c}, \sigma_{v_x,c}]$ for the object's state estimate. If we let itr be the number of iterations to get within ϵ of the steady-state covariance matrix, then the necessary time to observe an object to get arbitrary close to the steady-state is

$$T_{\text{measure}} = itr\Delta T. \tag{23}$$

Note that in practice we do not need many iterations to get close to the steady state. By studying equation (20a), we see that when $\sigma_{x,k} \to \infty$ then $a_1 \to \infty$ a single measurement is sufficient to move the position variance to $\sigma_{x,k+1} = r$.

Figure 1 illustrates the last two results. Here $q = 0.005\frac{m^2}{s^2}$, $r = 5m^2$, $\Delta T = 0.1s$, $\text{FOV}_{radius} = 150m$. The size of the confidence interval is 95%, which corresponds to $\chi_2^2 = 5.99$. This leads the minimum covariance matrix to be $[\sigma_{x,c}, \sigma_{xv_x,c}, \sigma_{v_x,c}] = [0.2187, 0.0489, 0.0224]$. The maximum period between visits is $T_{\text{NVP}} = 126.7s$. The time it takes to get a set of measurements within $\epsilon = 0.01$ of the steady-state covariance matrix is $T_{\text{measure}} = 110 \times \Delta T = 10.1s$.

The figure illustrates a simulation of σ_x^2 for an object starting at minimum variance and running for $T = T_{\text{freq}} + T_{\text{measure}} + T_{\text{freq}}$. The simulations is split into three intervals where it is first unobserved, observed, and then unobserved again.

IV. Area Size Estimates

The results of the last section enable us to calculate the maximum distance a single UAV can travel while keeping an object's position estimate error within a given confidence interval. We can then use this distance to estimate the size of the area a single UAV can monitor.

Let us assume that a UAV travels at constant velocity U and T_{NVP} is the period of the visitation period of an object from Theorem 2. The the maximum distance it can travel is easily calculated as
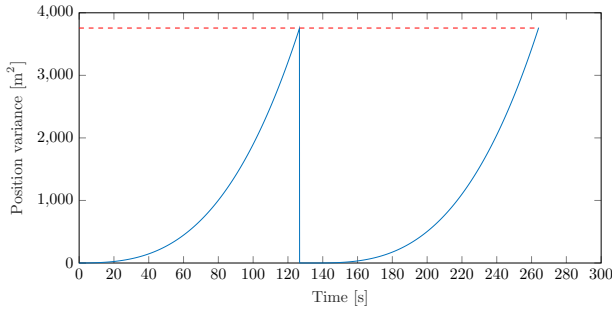
$$d_{\text{max}} = T_{\text{NVP}}U. \tag{24}$$

Fig. 1. Demonstration of Theorem 1 and 2. The blue solid line is the variance of the position estimate error of an object, and the red dotted line is the limit defined by $\frac{FOV_{\text{radius}}^2}{\chi_2^2}$

For example, consider a UAV traveling at $22\frac{m}{s}$ with the same sensor and FOV as used in the illustration at the end of Section III, Figure 1. Assume that the objects in the area also have the same properties as in that illustration. Then the UAV will be able to cover the distance

$$d_{\max} = 126.7 \times 22 = 2787.4m \qquad (25)$$

Let the minimum turning radius for the UAV be $105.8m$. Then, the area the UAV will be able to monitor could be a rectangular shape of size with areal 0.836km^2, as the one drawn in Figure 2.
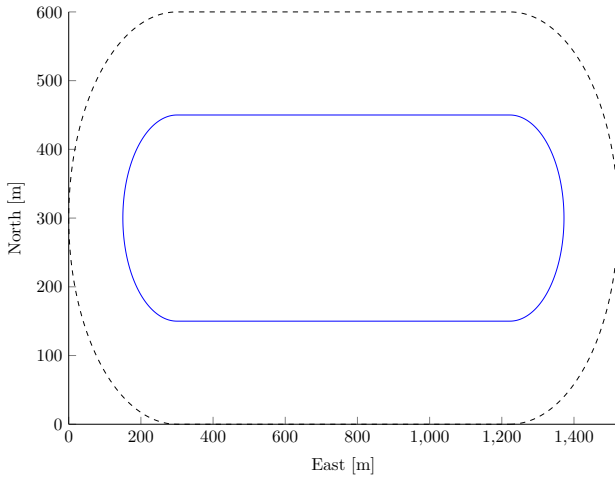

Fig. 2. Example path (blue solid curve) for the area (black dotted curve) a single UAV can monitor.

When calculating the area in Figure 2 we assume that the whole area must be visited with the given period. Therefore, it does not matter how many objects are within the area, since the UAV will pass every point with the necessary visitation period for each object. However, if we knew the number of objects to track, we could estimate a larger area the UAV could monitor.

To continue we will need some extra assumptions. In addition to assuming the number of objects known, we assume the object's positions are uniformly distributed and the UAV

is not subjected to the nonholonomic constraints of equation (2).

The necessary visitation period of each object will be the same as the case illustrated in Figure 2. This means that the maximal distance the UAV can travel is still given by equation (24). If we assumed that we had only two objects to track, we could calculate the probability distribution of distance between the objects. We could then use this probability distribution to calculate the probability that the distance will be longer than the maximal distance the UAV can travel and keep the variance of each object's position estimate error within a given confidence interval.

A challenge with this approach is that it will become increasingly difficult to calculate the probability distribution for the shortest distance between N objects. For two and three objects there will only be one possible route, but as the number of object increases the number of routs will increase exponentially. The problem of finding the shortest route is the traveling salesperson problem (TSP). Calculating the probability distribution will be a complex task. Instead, we will assume that the probability distribution for the shortest distance between N objects in a quadratic area with sides of length L will be normally distributed and can be approximate by running many Monte Carlo simulations.

To approximate the probability distribution of the shortest distance between N objects we solved 1000 TSP problems for each case of objects from 2 till 18. To solve the TSP problems, we use the CPLEX solver from IBM [19] implemented with YALMIP [20] in MATLAB R2016b. We use a mixed integer linear programming formulation for the TSP similar to Chen et al. [21].

Figure 3 and 4 plot the sample mean and standard deviation for the approximation of the probability distribution of the shortest distance between N objects. In addition, each plot also shows the 95% confidence interval for each property.
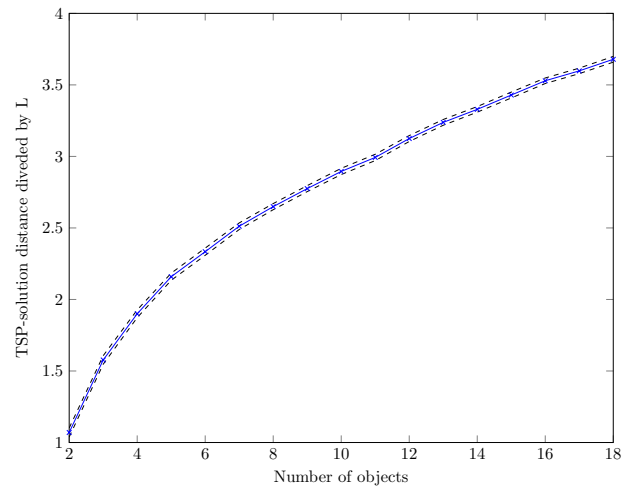

Fig. 3. The approximate mean of the shortest distance between objects divided by the side length of the quadrant L. The blue solid curve is the sample mean, with the 95% confidence interval indicated by black dotted curves.
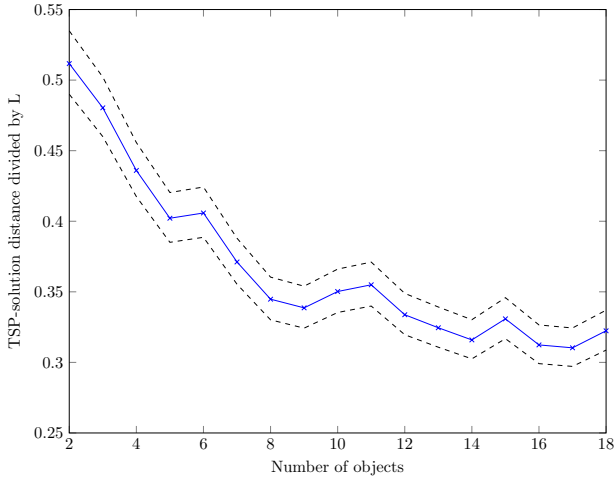
Fig. 4. The approximate standard deviation of the shortest distance between objects divided by side length L. The blue solid curve is the sample standard deviation, with the 95% confidence interval indicated by black dotted curves.
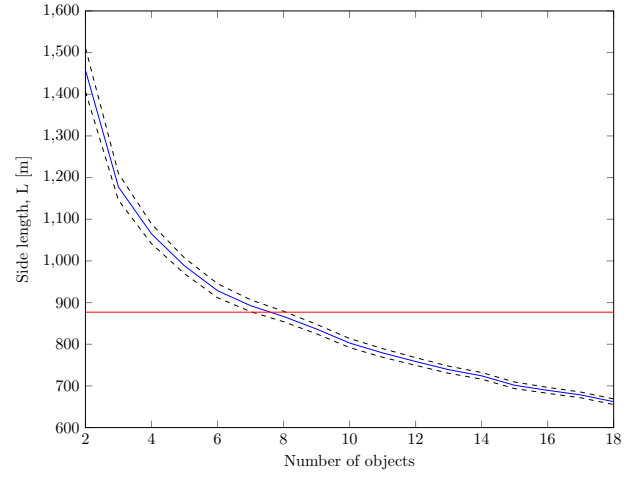

Fig. 5. Assuming a quadratic area, the length of the sides, calculated based on the maximal distance traveled for a single UAV given the number of objects. The solid blue curve is the side length, with the black dotted curves indicating the 95% confidence interval. The solid red line is the comparative side length for the area monitored by a UAV following the path given in Figure 2 ($\sqrt{836130}m = 914.4m$), if that area were quadratic.

We can use the approximate distributions to calculate an estimate on the size of the area we can monitor with a single UAV assuming we know the number of objects. For example, if we want it to be a 95% chance that the shortest distance between the objects is less than $d_{\max}$, we can calculate the side length of a quadratic area as

$$L = \frac{d_{\max}}{\hat{\mu}_i + 1.645\hat{\sigma}_i} \qquad (26)$$

where i is the number of objects we expect to find in an area, and $\hat{\mu}_i$ and $\hat{\sigma}_i$ are the approximate mean and standard deviation for the TSP solution distribution for i objects.

We can use the example from Figure 1 and 2 to calculate the maximal side length of a quadratic area given a 95% confidence interval for the number of objects from 2 till 18. The result is plotted in Figure 5. The blue curve is the side length of the area for the number of objects, the 95% confidence interval is indicated by the two dotted black curves. In addition, we have illustrated the side length for the area from Figure 2 if it were quadratic, which is $\sqrt{836130}m = 914.4m$, with a solid red line.

V. SIMULATION

To demonstrate the results from Section III and IV we ran 100 simulations of a single UAV following the path from Figure 2 with 100 objects in the area. The initial position and velocity of the objects as well as the noise sequences were randomized within a given interval for each simulation run. The remaining parameters were constant and are given in Table I. The confidence interval was chosen to be 95% ($\chi_2^2 = 5.99$).

Based on the simulation, we counted the number of times a redetected object was found within FOV and compared it to the number of times the error in position estimate increased beyond the FOV. The objects that moved outside of the patrol area of the UAV indicated by the dotted black curve in Figure

TABLE I
SIMULATION PARAMETERS

Parameter	Value	Unit
UAV	1 units	
$(x_0,y_0,\text{heading})$	(300,150,0)	(m,m,rad)
Minimum turning radius	105.8	m
FOV$_{radius}$	150	m
Velocity	22	m/s
Objects	100 units	
x_0	$\in[-350,1850\ ]$	m
y_0	$\in[-350,950]$	m
v_x	$\in[-1,1]$	m/s
v_y	$\in[-1,1]$	m/s
Observer		
Measurement period, ΔT	0.1	s
Process noise variance, q	0.005	m/s^2
Measurement noise variance, r	5	m^2
χ_2^2	5.99	
Simulation		
Simulation length, T	500	s

2 were ignored. The results are illustrated in Figure 6 and 7. Overall the UAV managed to redetect discovered objects with a success rate of 97.60%.

VI. DISCUSSION

When we study Figure 6 and 7 we realize that in several cases the UAV does not visit the objects with a period given by T_{NVP} from equation (21). The reason is that the UAV does not fulfill the assumption of measuring at the estimated position of each object, instead it only measures at each position in the area with period, T_{NVP}. This means that when following the simple path from Figure 2, the movement of the objects are not considered. However, as we can see from Figure 6 that for most objects the visitations occur with a period close to T_{NVP}.
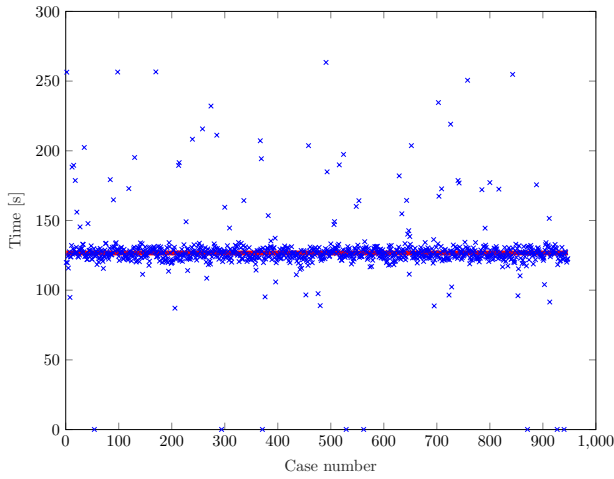
Fig. 6. The visitation period for the successful cases redetection of objects. Each case of redetection is indicated by a blue X. The T_{NVP} from equation (21) is drawn as a solid red line. Only the first 1000 cases of redetection are shown for clarity of the figure.
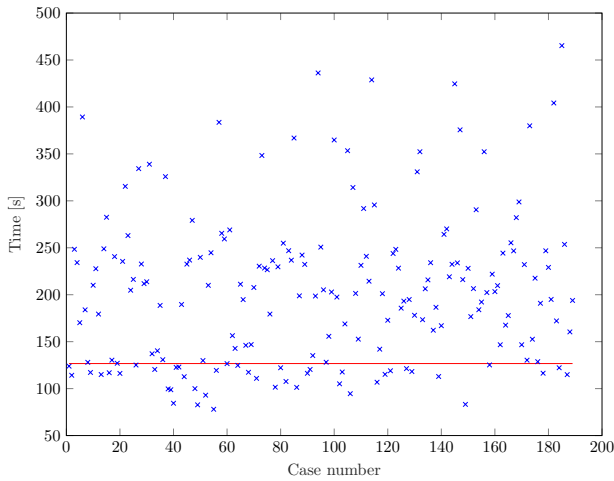

Fig. 7. The time when the error in the estimated position of an object exceeds the FOV of the UAV. Each case is marked with a blue X. The T_{freq} from equation (21) is drawn as a solid red line

From the chosen confidence interval of 95% we would expect to redetect objects within FOV in 95% of the cases. However, the UAV managed to redetect the objects with a success rate of 97.6%. There are two factors that effects the success rate. First, as already mention the UAV does not take into consideration the movement of the objects. An algorithm that guarantee that each object position estimate is visited within a time span of T_{NVP} will have a worst case redetection rate of 95%. When the UAV follows the path from Figure 2, the estimated position of the objects are not considered and thus no such guarantee can be given. When we study the cases where the objects moved outside FOV, illustrated in Figure 7, for most of them the UAV failed to return within the given time span T_{NVP}. The second factor that increases the success rate comes from ignoring the objects that moves outside the patrol area given by the dotted black curve in Figure 2.

Finally, the result at the end of Section 5 enables us to select a path planning algorithm based on the size and the expected number of objects in the area. As the number of objects increases an optimization algorithm for searching and tracking objects will perform increasingly worse compared to following a simple path like the one illustrated in Figure 2.

VII. CONCLUSION AND FURTHER WORK

In this paper we have derived a performance bound for the variance of the position estimate error of objects following a constant velocity model with noise. This performance bound have then been used to calculate the necessary visitation frequency of an object, such that the probability of the error in the position estimate, to increase beyond the FOV, is within a given confidence interval. We calculate the size of the area assuming that a UAV need to monitor the whole area with the given visitation period. In addition, we have also approximated the probability distributions for TSP-solutions with different number of objects. We have used this to calculate an estimate of the area size a UAV can monitor when only needing to visit the objects with the given visitation period. We have demonstrated a single UAV monitoring a limited area in Monte Carlo simulations with 100 objects. Finally, based on the results we have been able to recommend a path planning strategy based on the size and number of objects in the area.

Future work:

- Extend the results with the probability of detection. Even when an objects is within FOV of a UAV it is not guaranteed to get a measurement of the object.
- Generalize the result with a more complicated measurement model for example coupling between north/east position and velocity.
- Develop similar result for multiple UAVs.
- Create an algorithm based on the visiting frequency, T_{NVP}, for searching and tracking objects with a UAV.
- Create and perform experimental setup to validate the results.

REFERENCES

[1] K. Valavanis and G. Vachtsevanos, "UAV applications: Introduction," *Handbook of Unmanned Aerial Vehicles*, pp. 2639–2641, 2015.

[2] A. Albert and L. Imsland, "Mobile sensor path planning for iceberg monitoring using a MILP framework," in *ICINCO 2015 - 12th International Conference on Informatics in Control, Automation and Robotics, Proceedings*, vol. 1, 2015, pp. 131–138.

[3] L. Merino, J. R. Martínez-de Dios, and A. Ollero, "Cooperative unmanned aerial systems for fire detection, monitoring, and extinguishing," in *Handbook of Unmanned Aerial Vehicles*. Springer, 2015, pp. 2693–2722.

[4] A. R. Girard, A. S. Howell, and J. K. Hedrick, "Border patrol and surveillance missions using multiple unmanned air vehicles," in *Decision and Control, 2004. CDC. 43rd IEEE Conference on*, vol. 1. IEEE, 2004, pp. 620–625.

[5] C. Goerzen, Z. Kong, and B. Mettler, "A survey of motion planning algorithms from the perspective of autonomous uav guidance," in *Selected papers from the 2nd International Symposium on UAVs, Reno, Nevada, USA June 8–10, 2009*. Springer, 2009, pp. 65–100.

[6] M. Hernandez, "Performance bounds for target tracking: computationally efficient formulations and associated applications," *Integrated Tracking, Classification, and Sensor Management: Theory and Applications*, pp. 255–310, 2012.

[7] P. Tichavsky, C. H. Muravchik, and A. Nehorai, "Posterior cramér-rao bounds for discrete-time nonlinear filtering," *IEEE Transactions on signal processing*, vol. 46, no. 5, pp. 1386–1396, 1998.

[8] Y. Kim and H. Bang, "Airborne multisensor management for multitarget tracking," in *Unmanned Aircraft Systems (ICUAS), 2015 International Conference on*. IEEE, 2015, pp. 751–756.

[9] B. Ristic, S. Zollo, and S. Arulampalam, "Performance bounds for manoeuvring target tracking using asynchronous multi-platform angle-only measurements," in *Proceedings of the 4th International Conference on Information Fusion*. Citeseer, 2001.

[10] R. Tharmarasa, T. Kirubarajan, M. L. Hernandez, and A. Sinha, "Pcrlb-based multisensor array management for multitarget tracking," *IEEE Transactions on Aerospace and Electronic Systems*, vol. 43, no. 2, 2007.

[11] M. L. Hernandez, "Adaptive horizon sensor resource management: validating the core concept," in *Optical Engineering+ Applications*. International Society for Optics and Photonics, 2007, pp. 66 990V–66 990V.

[12] X. R. Li, R. R. Pitre, V. P. Jilkov, and H. Chen, "A new performance metric for search and track missions," in *Information Fusion, 2009. FUSION'09. 12th International Conference on*. IEEE, 2009, pp. 1100–1107.

[13] R. R. Pitre, X. R. Li, and R. Delbalzo, "Uav route planning for joint search and track missions—an information-value approach," *IEEE Transactions on Aerospace and Electronic Systems*, vol. 48, no. 3, pp. 2551–2565, 2012.

[14] M. Raap, M. Moll, M. Zsifkovits, and S. Pickl, "Utilizing dual information for moving target search trajectory optimization," in *OASIcs-OpenAccess Series in Informatics*, vol. 50. Schloss Dagstuhl-Leibniz-Zentrum fuer Informatik, 2016.

[15] X. Tian, Y. Bar-Shalom, K. Pattipati, and A. Sinha, "Surveillance by multiple cooperative uavs in adversarial environments," in *SPIE Defense and Security Symposium*. International Society for Optics and Photonics, 2008, pp. 69 691E–69 691E.

[16] F. Leira, T. A. Johansen, and T. I. Fossen, "Automatic detection, classification and tracking of objects in the ocean surface from uavs using a thermal camera," in *IEEE Aerospace Conference*, 2015.

[17] A. Gelb, *Applied optimal estimation*. MIT press, 1974.

[18] R. S. Irving, *Integers, polynomials, and rings: a course in algebra*. Springer Science & Business Media, 2003.

[19] "IBM Ilog CPLEX optimization studio CPLEX users manual," http://www.ibm.com, 2015, accessed: 2015-09-12.

[20] J. Löfberg, "YALMIP : A toolbox for modeling and optimization in MATLAB," in *Proceedings of the CACSD Conference*, 2004.

[21] D.-S. Chen, R. G. Batson, and Y. Dang, *Applied integer programming: modeling and solution*. John Wiley & Sons, 2010.